ARTICLE

Stable inhibition of choroidal neovascularization by adeno-associated virus 2/8-vectored bispecific molecules

Tinghui Bai[1,4], Bohao Cui[1,4], Man Xing[2], Siyue Chen[1], Yanfang Zhu[1], Dongxue Lin[1], Yingying Guo[2], Mei Du[1,3], Xiaohong Wang[1,3]✉, Dongming Zhou[2]✉ and Hua Yan[1]✉

Neovascular age-related macular degeneration (nAMD) causes severe visual impairment. Pigment epithelium-derived factor (PEDF), soluble CD59 (sCD59), and soluble fms-like tyrosine kinase-1 (sFLT-1) are potential therapeutic agents for nAMD, which target angiogenesis and the complement system. Using the AAV2/8 vector, two bi-target gene therapy agents, AAV2/8-PEDF-P2A-sCD59 and AAV2/8-sFLT-1-P2A-sCD59, were generated, and their therapeutic efficacy was investigated in laser-induced choroidal neovascularization (CNV) and *Vldlr*$^{-/-}$ mouse models. After a single injection, AAV2/8-mediated gene expression was maintained at high levels in the retina for two months. Both AAV2/8-PEDF-P2A-sCD59 and AAV2/8-sFLT-1-P2A-sCD59 significantly reduced CNV development for an extended period without side effects and provided efficacy similar to two injections of current anti-vascular endothelial growth factor monotherapy. Mechanistically, these agents suppressed the extracellular signal-regulated kinase and nuclear factor-κB pathways, resulting in anti-angiogenic activity. This study demonstrated the safety and long-lasting effects of AAV2/8-PEDF-P2A-sCD59 and AAV2/8-sFLT-1-P2A-sCD59 in CNV treatment, providing a promising therapeutic strategy for nAMD.

Gene Therapy (2024) 31:511–523; https://doi.org/10.1038/s41434-024-00461-1

INTRODUCTION

Age-related macular degeneration (AMD) is the primary cause of severe visual impairment in individuals older than 55 years. With an aging population, AMD affected 196 million people worldwide in 2020, which will increase to 288 million by 2040 [1]. AMD may be divided into two major types: non-neovascular and neovascular AMD (nAMD). nAMD is characterized by choroidal neovascularization (CNV) in which new vessels rupture and leak easily, leading to fluid accumulation and vision loss [2].

Anti-vascular endothelial growth factor (anti-VEGF) therapy is the first-line treatment for nAMD. Multiple intravitreal injections of anti-VEGF agents are required for treatment, which burdens the patient's quality of life and may result in complications, such as endophthalmitis and retinal detachment [3–5]. Because the pathogenic factors of nAMD are complex, the efficacy of the anti-VEGF agent varies from person to person. Studies on nAMD show that after 1 year of anti-VEGF therapy, 35.2%-70.9% of patients still have retinal fluid [6–8]. Therefore, the development of long-acting and multitarget compounds is required to enhance therapeutic effects in nAMD.

Gene therapy is a promising strategy for nAMD treatment. Recombinant adeno-associated virus (rAAV) is the leading platform for gene therapy owing to its long transgene expression, low immunogenicity, non-pathogenicity, and broad tropism. Furthermore, rAAV rarely integrates into the host chromosome and transduces both dividing and non-dividing cells [9, 10]. ADVM-022 is a gene therapy agent using AAV.7m8 with aflibercept (AAV.7m8-AFB) to inhibit nAMD. In a Phase I clinical trial, a single injection of ADVM-022 was comparable to anti-VEGF therapy for over 24 weeks, without common complications [11]. RGX-314 was designed using an AAV8 vector that delivered an anti-VEGF antibody fragment. Phase I/II clinical trials of RGX-314 have revealed a reduction in the anti-VEGF treatment burden, stable visual acuity (VA), and decreased central subfield thickness [12]. AAV2/8 is also an ideal gene therapy vector that effectively transduces the retina and expresses transgenes at high levels [13].

As pigment epithelium-derived factor (PEDF), soluble CD59 (sCD59), and soluble fms-like tyrosine kinase-1 (sFLT-1) are potential therapeutic agents for nAMD that target angiogenesis and the complement system, two bi-target gene therapy agents were generated using AAV2/8, AAV2/8-PEDF-P2A-sCD59, and AAV2/8-sFLT-1-P2A-sCD59 [14–17]. Laser-induced CNV and very low-density lipoprotein receptor (*Vldlr*)$^{-/-}$ mouse models were established to detect the dual inhibitory effects of the agents on neovascularization. The retinal safety of the agents was evaluated using optical coherence tomography (OCT) and terminal deoxynucleotidyl transferase dUTP nick end labeling (TUNEL) assays. After a single injection, the two dual inhibitors exhibited similar long-term efficiency compared with two injections of anti-VEGF monotherapy (Conbercept).

[1]Department of Ophthalmology, Tianjin Medical University General Hospital, Ministry of Education International Joint Laboratory of Ocular Diseases, Tianjin Key Laboratory of Ocular Trauma, Tianjin Institute of Eye Health and Eye Diseases, China-UK "Belt and Road" Ophthalmology Joint Laboratory, Tianjin, China. [2]Department of Pathogen Biology, School of Basic Medical Sciences, Tianjin Medical University, Tianjin, China. [3]Department of Pharmacology, Tianjin Key Laboratory of Inflammation Biology, the Province and Ministry Co-sponsored Collaborative Innovation Center for Medical Epigenetics, School of Basic Medical Sciences, Tianjin Medical University, Tianjin, China. [4]These authors contributed equally: Tinghui Bai, Bohao Cui ✉email: xiaohongwang@tmu.edu.cn; zhoudongming@tmu.edu.cn; zyyyanhua@tmu.edu.cn

Received: 28 December 2023 Revised: 14 June 2024 Accepted: 25 June 2024
Published online: 3 July 2024

MATERIALS AND METHODS

Vector production

The soluble variant of the VEGF receptor-1 (sFLT-1) was designed using *Homo sapiens* Flt-1 (NM_001159920, NCBI Reference Sequence, NIH). PEDF was designed using *Homo sapiens* serpin family F member 1 (NM_001329903, NCBI Reference Sequence, NIH). sCD59 was designed using the *Homo sapiens* CD59 molecule (NM_000611, NCBI Reference Sequence, NIH). A P2A liner was used to connect sFLT-1/PEDF and sCD59. The multigenic cassette was inserted into pAAV-MCS (NCBI: taxonomy id 167882) under the control of cytomegalovirus. The AAV2/8 vectors were generated by transfecting HEK-293T cells with the AAV2/8-PEDF-P2A-sCD59/AAV2/8-sFLT-1-P2A-sCD59 plasmid, pHelper (NCBI: taxonomy id 161366), and pAAV2/8 (Addgene plasmid #112864) capsid plasmids and purified using iodixanol density gradient ultracentrifugation. AAV viruses were titrated using quantitative reverse transcription-polymerase chain reaction (qRT-PCR).

Cell culture

HEK-293T cells and BV2 microglial cells were purchased from the Shanghai Institute of Cell Biology of the Chinese Academy of Sciences (Shanghai, China). The HEK-293T and BV2 cells were grown in Dulbecco's modified Eagle's medium (catalog no. SH30243.01; Cytiva, Marlborough, MA, USA) supplemented with 10% fetal bovine serum (FBS, catalog # MN221012; EallBio, Beijing, China) and 1% penicillin/streptomycin (catalog #. C100C5; NCM Biotech, Suzhou, China) and cultured in 5% CO_2 and 37 °C.

Animals

Male C57BL/6J mice, 6–8 weeks old, were purchased from Beijing Vital River Laboratory Animal Technology and housed under a 12-h light/12-h dark cycle in the animal facility at Tianjin Medical University. All animal experiments were approved by the Institutional Animal Care and Use Committee of Tianjin Medical University (TMUaMEC 2022006).

Intravitreal injection

Mice were anesthetized using isoflurane (1.5–2 mL min^{-1}). A 34-gauge Hamilton syringe (catalog no. 7633-01; Hamilton, Reno, Nevada, USA) was inserted into the vitreous behind the limbus of the cornea through a small puncture created using a 30-gauge needle. Mice were randomly divided into four groups and injected with 2 μL of AAV2/8-ZsGreen (1.8 $\times 10^9$ vg μL^{-1}), AAV2/8-PEDF-P2A-sCD59 (1.8 $\times 10^9$ vg μL^{-1}), AAV2/8-sFLT-1-P2A-sCD59 (1.8 $\times 10^9$ vg μL^{-1}), PBS or Conbercept (10 mg mL^{-1}). Before and after injections, 0.5% levofloxacin eye drops were administered to prevent infection. Animals affected by injection issues, such as intraocular hemorrhage, were excluded from the analysis.

Laser-induced CNV

Mice were anesthetized using intraperitoneal injection of 1.25% tribromoethanol (0.2 mL/10 g mouse). The pupils were dilated with tropicamide eye drops (5 mg mL^{-1}). YAG laser photocoagulation (LB-002088 REV B, Lumenis, San Jose, CA, USA) was performed to generate four laser burns per eye around the optic disc (one per quadrant) at 100 μm spot size, 0.15 s duration, 200 mW power, as previously described [18]. Bubble formation in the laser burn spots successfully indicated rupture of Bruch's membrane. Treated eyes were smeared with levofloxacin hydrochloride capsules to prevent infection.

FFA

FFA was performed using Heidelberg confocal retinal angiography at 7 and 14 days after laser photocoagulation. Fundus images were obtained 3–5 min after intraperitoneal administration of fluorescein sodium (10%, 0.01 mL/5 g body weight). The leakage area of the CNV lesion was analyzed using ImageJ software by two experienced examiners who were blinded to the experimental groups.

Optical coherence tomography

Four weeks after injection, retinal thickness was assessed using SD-OCT (Micron IV, Phoenix Research Labs, Pleasanton, CA, USA). Circular volume scans were centered on the optic disc to evaluate the retinal structure. OCT images were analyzed using ImageJ software and manually segmented by masked graders.

Immunofluorescence staining

Mouse eyes were enucleated and fixed with 4% paraformaldehyde for 1-2 h at room temperature. After removing the anterior segment, the RPE-choroid complexes or retinas were collected and permeabilized with 1% Triton X/PBS for 12 h at 4 °C. Then, the RPE-choroid complexes or retina were incubated with a blocking solution [2% bovine serum albumin (Solarbio, Beijing, China) and 0.3% Triton X-100 (Solarbio) in PBS] for 12 h at 4 °C. The complexes or retinas were incubated with a blocking solution containing primary hamster anti-mouse CD31 monoclonal antibody (catalog no. MAB1398Z; Millipore, Boston, MA, USA), F4/80 (catalog no. 30325 S; Cell Signaling Technology, Boston, MA, USA), or anti-C5b-9 antibody (catalog no. ab55811; Abcam, Cambridge, MA, USA) for 48 h at 4 °C. After incubation with primary antibody, the eyecups were incubated with Alexa Fluor 488-conjugated secondary antibodies (1:400; catalog no. 111-545-003; Jackson ImmunoResearch, Suffolk, UK) and Alexa Fluor 594-conjugated secondary antibodies (1:400; catalog no. 127-585-099; Jackson ImmunoResearch) for 2 h at room temperature and then washed with 0.1% Triton X/PBS three times. Finally, the RPE-choroid complex or retina was flattened on microscopic slides and observed using a laser-scanning confocal fluorescence microscope.

The retinal neovascularization area was measured using ImageJ software, and z stacks were 3D reconstructed using Imaris X64 9.0.1 software. The CNV area was measured using Imaris X64 9.0.1 software.

Western blotting

Proteins were extracted from the cells or RPE-choroid complexes. Equivalent amounts of protein were loaded onto 10–15% sodium dodecyl-sulfate-polyacrylamide gels and transferred onto polyvinylidene difluoride membranes. Membranes were blocked with 5% skim milk in Tris-buffered saline containing 0.1% Tween-20 (TBST) at room temperature for 2 h. Membranes were incubated with the following antibodies overnight at 4 °C: anti-PEDF (catalog no. 11104-RP02; Sino Biological, Beijing, China), anti-VEGF receptor 1 (catalog no. 36-1100; Invitrogen, Waltham, MA, USA), anti-CD59 (catalog no. 12474-RP02; Sino Biological), anti-p-ERK1/2 (catalog no. 4370; Cell Signaling Technology), anti-ERK1/2 (catalog no. 9102; Cell Signaling Technology), anti-iNOS (catalog no. ab3523; Abcam), anti-IL-1β (catalog no. 12507; Cell Signaling Technology), anti-NF-κB p65 (catalog no. 8242; Cell Signaling Technology), anti-phospho-NF-κB p65 (catalog no. 3033; Cell Signaling Technology), or anti-NF-κB1 p105 (catalog no. 13586; Cell Signaling Technology). After washing with TBST, membranes were incubated with horseradish peroxidase-conjugated secondary goat anti-rabbit antibodies (catalog no. ab6721; Abcam) at room temperature for 2 h. Membranes were washed with TBST three times, and protein levels were recorded using an enhanced chemiluminescence kit (catalog no. 32106; Thermo Fisher Scientific, Waltham, MA, USA) and a molecular imaging system.

qRT-PCR

The total RNA of the retina and RPE-choroid complex was isolated and purified from mouse eyes. RNA was reverse transcribed into cDNA using the RevertAid First Strand cDNA Synthesis Kit (catalog no. K1621; Thermo Fisher Scientific). qRT-PCR was performed using 2 × RealStar Power SYBR qPCR Mix (catalog no. A312; GeneStar, Beijing, China) with PEDF primers (F: 5′-caaagagatccccgacgaga; R: 5′-gggcgattttacagctcagg), sCD59 primers (F: 5′-ctgcctgatcaccaaagcc; R: 5′-agctgctcgttaaagttgca), and sFLT-1 primers (F: 5′-ctgagcatcaagcagagcaa; R: 5′-ctgtggttgtggttgcagg). Mouse β-actin was used as a reference gene (F: 5′-ggctgtattcccctccatcg; R: 5′-ccagttggtaa-caatgccatgt). Relative expression levels of PEDF, sCD59, or sFLT-1 were calculated using the ΔΔCt method, as previously described [19].

TUNEL assay

Apoptosis in mouse retinal cells was detected with a TUNEL assay using the One Step TUNEL Apoptosis Assay Kit (catalog no. C1089; Beyotime Biotechnology, Shanghai, China). Mouse frozen sections of 10–20 μm thickness were washed using 1× PBS three times and permeabilized in 0.5% Triton X-100. Eye sections from wild-type mice treated with DNase I (1 ug ml^{-1}, 10 min at room temperature) to induce DNA strand breaks served as positive controls. The cryosections were incubated with a TUNEL reaction mixture at 37 °C in the dark for 1 h. After rinsing three times with PBS, the tissues were mounted with Fluoroshield containing DAPI (catalog no. ab6721; Abcam) for nuclear staining and imaging using a laser-scanning confocal fluorescence microscope.

RNA sequencing and bioinformatics analysis

Each sample was pooled using two retinal-RPE-choroid complexes from one mouse. RNA was extracted, and its quality was analyzed using an Agilent 2100 Bioanalyzer (Agilent Technologies, Santa Clara, CA, USA).

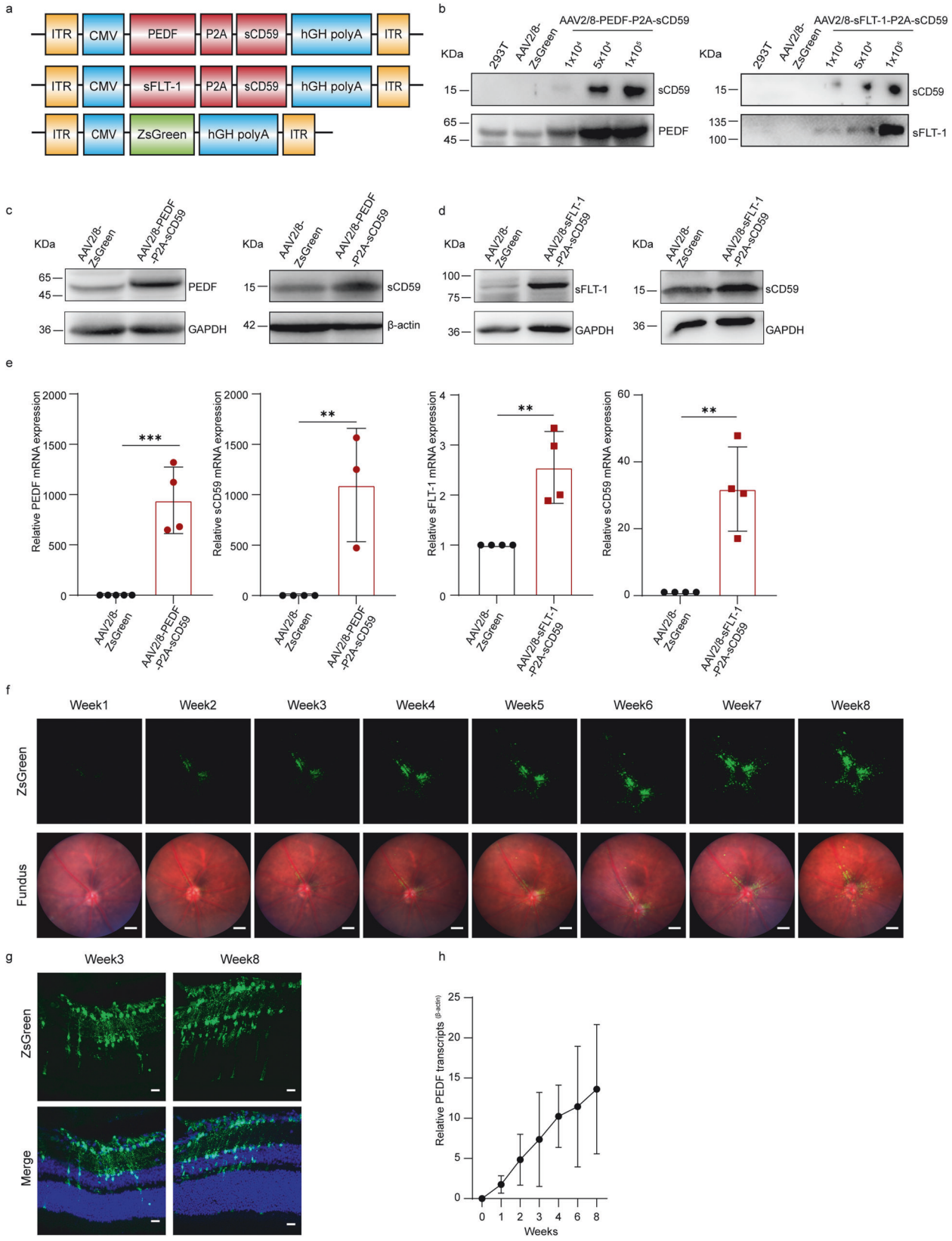

Sequencing was performed at Majorbio (Beijing, China) on an Illumina NovaSeq 6000 according to the manufacturer's instructions (Illumina, San Diego, CA, USA). Four AAV2/8-ZsGreen, four AAV2/8-PEDF-P2A-sCD59, five AAV2/8-sFLT-1-P2A-sCD59, and five Conbercept mice were used. Genes with an absolute value of the $\log_2$ fold change ≥1 and $P \leq 0.05$ were considered to be differently expressed. Enrichment analyses were performed using the Molecular Signatures Database (MSigDB) in Enrichr (https://maayanlab.cloud/Enrichr/) [20–22]. For gene set enrichment analysis (GSEA), gene sets were acquired from the MSigDB, and GSEA_4.1.0 software was used [23–25].

Fig. 1 The efficiency of intravitreal AAV2/8-mediated gene delivery in vitro and in vivo. a Map of AAV2/8 vectors expressing pigment epithelium-derived factor (PEDF), soluble fms-like tyrosine kinase-1 (sFLT-1), and soluble CD59 (sCD59). The sFLT-1 and sCD59 genes and the PEDF and sCD59 genes were connected using a P2A linker. **b** Western blotting from HEK-293T cells infected with AAV2/8-ZsGreen, AAV2/8-PEDF-P2A-sCD59, and AAV2/8-sFLT-1-P2A-sCD59 at different multiplicity of infection (MOI). **c** Western blotting of PEDF and sCD59 in the retina-retinal pigment epithelium (RPE)-choroid complex of mice three weeks after injection of AAV2/8-ZsGreen/AAV2/8-PEDF-P2A-sCD59. **d** Western blotting of sFLT-1 and sCD59 in the retina-RPE-choroid complex of mice three weeks after injection of AAV2/8-ZsGreen/AAV2/8-sFLT-1-P2A-sCD59. **e** Relative mRNA expression of PEDF, sFLT-1 and sCD59 in the retina-RPE-choroid complex of mice three weeks after injection of AAV2/8-PEDF-P2A-sCD59/AAV2/8-sFLT-1-P2A-sCD59. (n = 3–5 mice per group). **f** AAV2/8-ZsGreen expression detected at similar intensities by live fundus photography at different time points from 1 week to 8 weeks post-intravitreal injection. Scale bars, 300 μm. **g** Cryosections of eyes at week 3 and week 8 after AAV2/8-ZsGreen injection. Scale bars, 20 μm. **h** Relative PEDF mRNA expression in AAV2/8-PEDF-P2A-sCD59-treated mouse retina from 1 week to 8 weeks post-intravitreal injection (n = 4–9 mice per group). Data are analyzed using the Student's *t* test between groups in **e** (*$P < 0.05$, **$P < 0.01$, ***$P < 0.001$, ****$P < 0.0001$). Data are presented as mean ± SD.

Statistical analysis

Data were analyzed using GraphPad Prism 9.4.0. The graphs are presented using the mean ± SD of at least three independent experiments. Data comparison of two groups was performed using Student's *t* test (two-tailed). One-way analysis of variance was used to analyze normally distributed variables among multiple groups, followed by Tukey's post-hoc test. $P < 0.05$ was considered significantly different. MsigDB enrichment analysis was performed to identify the affected biological pathways.

RESULTS

The efficiency of intravitreal AAV2/8-mediated gene delivery in vitro and in vivo

Two bi-target gene therapy agents, AAV2/8-PEDF-P2A-sCD59 and AAV2/8-sFLT-1-P2A-sCD59, were designed and connected to a P2A cleavable linker. AAV2/8-ZsGreen was constructed as a negative control (Fig. 1a). HEK-293T cells were transfected with AAV2/8-PEDF-P2A-sCD59 or AAV2/8-sFLT-1-P2A-sCD59 to evaluate the expression of sFLT-1, PEDF, and sCD59. The PEDF protein was detected in the cell lysate and medium at 50 KDa. The secreted proteins, sFLT-1, and sCD59, were detected mainly in the culture medium at 100–135 KDa and 10–15 KDa, respectively (Fig. 1b).

AAV2/8-PEDF-P2A-sCD59, AAV2/8-sFLT-1-P2A-sCD59, and AAV2/8-ZsGreen were injected intravitreally to examine the expression of PEDF, sFLT-1, and sCD59. Target protein levels were markedly elevated in the AAV2/8-PEDF-P2A-sCD59- and AAV2/8-sFLT-1-P2A-sCD59-injected groups (Fig. 1c, d). The mRNA levels of PEDF and sCD59 were significantly higher in AAV2/8-PEDF-P2A-sCD59-injected eyes than in AAV2/8-ZsGreen-injected eyes. sFLT-1 and sCD59 expression was also increased in AAV2/8-sFLT-1-P2A-sCD59-injected eyes (Fig. 1e).

To evaluate the kinetics of target gene expression, AAV2/8-ZsGreen was injected into the vitreous body at 3.6×10^9 genome copies per eye. ZsGreen signaling was examined at 1-week post-administration and gradually increased over 8 weeks (Fig. 1f). Cryosections from eyes indicated that the ZsGreen expression could be detected in retinal ganglion cell layer, inner plexiform layer, inner nuclear layer, outer plexiform layer and outer nuclear layer (Fig. 1g). Next, AAV2/8-PEDF-P2A-sCD59 was delivered into mouse eyes, and the transcript levels of PEDF from week 1 to week 8 were detected using qPCR. This result was consistent with the tendency of ZsGreen expression to be conferred by AAV2/8-ZsGreen. The PEDF mRNA level increased slowly in the first week but increased to a relatively high level at weeks 2–4 and continued to increase until week 8, the endpoint of the experiment (Fig. 1h). These results illustrated that the dual inhibitors AAV2/8-PEDF-P2A-sCD59 and AAV2/8-sFLT-1-P2A-sCD59 were successfully constructed with robust expression at 2–3 weeks post-delivery and were maintained for at least 2 months.

Treatment with AAV2/8-mediated genes via intravitreal delivery effectively inhibited laser-induced CNV

To evaluate the potential of AAV2/8-mediated gene therapy, a laser-induced CNV mouse model was used to mimic nAMD pathogenesis [26]. Mice received intravitreal injections of AAV2/8-PEDF-P2A-sCD59, AAV2/8-sFLT-1-P2A-sCD59, AAV2/8-ZsGreen, or PBS three weeks prior to laser-induced injury (Fig. 2a). Conbercept, an anti-VEGF medicine widely used for patients with nAMD, was used as a positive control. Fundus fluorescein angiography (FFA) was performed to evaluate the leakage area of the CNV 7 and 14 days after laser treatment (Fig. 2b). Compared with PBS and AAV2/8-ZsGreen group, eyes injected with AAV2/8-PEDF-P2A-sCD59, AAV2/8-sFLT-1-P2A-sCD59 showed significant reductions in the vascular leakage area at day 7 and 14 (Fig. 2c, d). Compared with the AAV2/8-ZsGreen group, reductions of 47.0% and 44.8% in mean leakage area were achieved in the AAV2/8-PEDF-P2A-sCD59 ($P < 0.0001$) and AAV2/8-sFLT-1-P2A-sCD59 group ($P < 0.0001$) at day 7. On day 14, 45.8% and 36.0% were detected in the AAV2/8-PEDF-P2A-sCD59 ($P = 0.0013$) and AAV2/8-sFLT-1-P2A-sCD59 group ($P = 0.0217$). No statistical differences were observed among the AAV2/8-PEDF-P2A-sCD59, AAV2/8-sFLT-1-P2A-sCD59, and Conbercept groups (Fig. 2c, d).

The complement terminal C5b-9 complex, also known as the membrane attack complex (MAC), is a collective terminal effector of the classical, lectin, and alternative complement pathways. CD31 and C5b-9 were stained on the flat mount to evaluate whether AAV vectors exerted anti-angiogenic and anti-complement effects in the CNV model. The flat mount was heavily stained with CD31 and MAC at the laser speckle in the AAV2/8-ZsGreen group three days after laser coagulation (Fig. 2e). CD31 positive volume measurements showed significant reductions of neovascularization in mice injected with AAV2/8-PEDF-P2A-sCD59 (42.7%, $P < 0.0036$) and AAV2/8-sFLT-1-P2A-sCD59 (33.7%, $P < 0.0415$; Fig. 2f). Significant decreases in MAC deposition on flat mounts were observed after delivery of AAV2/8-PEDF-P2A-sCD59 (50.8%, $P < 0.0001$) and AAV2/8-sFLT-1-P2A-sCD59 (51.4%, $P < 0.0001$; Fig. 2g).

AAV2/8-mediated gene therapy resulted in long-term inhibition of laser-induced CNV

To inspect long-term antineovascular efficiency, repeat laser induction in the same eyes after the first laser induction was performed (Fig. 3a), as previously described [27]. In the positive control group, a second injection of Conbercept was administered immediately after the second laser induction. FFA was applied on days 7 and 14 to examine the angiogenic leakage area (Fig. 3b). On day 7, significant decreases of 34.3%, 33.5%, and 32.9% in the mean leakage area were noted in the AAV2/8-PEDF-P2A-sCD59 ($P = 0.0081$), AAV2/8-sFLT-1-P2A-sCD59 ($P = 0.0122$), and Conbercept ($P = 0.0249$) groups, respectively, in comparison with that in the AAV2/8-ZsGreen group (Fig. 3c). On day 14, significant reductions of 41.6%, 39.7%, 37.8% were observed in mice administered AAV2/8-PEDF-P2A-sCD59 ($P = 0.0004$), AAV2/8-sFLT-1-P2A-sCD59 ($P = 0.0008$), and Conbercept ($P = 0.0031$) compared to AAV2/8-ZsGreen group (Fig. 3d). Furthermore, there were no statistical differences among the AAV2/8-PEDF-P2A-sCD59, AAV2/8-sFLT-1-P2A-sCD59 and the Conbercept groups at any time point.

A flat mount of the retinal pigment epithelium (RPE)-choroid complex was stained with CD31 and F4/80 to detect the volume

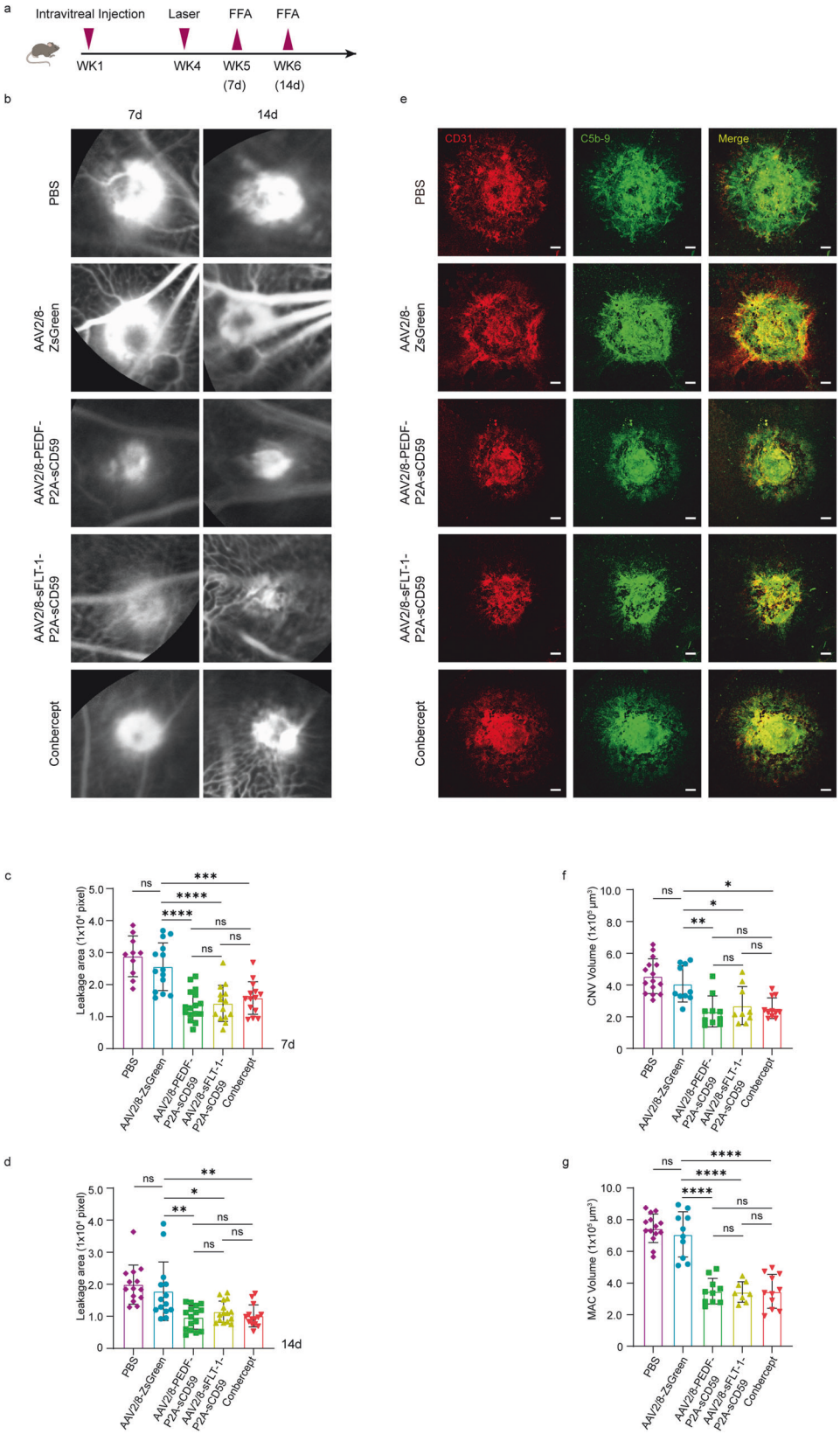

of CNV and macrophage infiltration, respectively (Fig. 3b). Compared to AAV2/8-ZsGreen group, significant neovascularization volume reductions of 48.2%, 47.9%, 56.3% were evaluated in AAV2/8-PEDF-P2A-sCD59 ($P < 0.0001$), AAV2/8-sFLT-1-P2A-sCD59 ($P < 0.0001$), and Conbercept ($P < 0.0001$) group 14 days after laser induction (Fig. 3e). Macrophages are the main inflammatory cells that infiltrate eyes with nAMD [28, 29]. Macrophage infiltration was significantly reduced in AAV2/8-PEDF-P2A-sCD59 (54.4%,

Fig. 2 Treatment with AAV2/8-mediated genes via intravitreal delivery effectively inhibited laser-induced CNV. a Sequential order of intravitreal injections, CNV induction, and analysis. **b** Representative fundus fluorescein angiography (FFA) images showing vascular leakage from mice undergoing indicated treatment after laser-induced CNV at days 7 and 14. **c** Quantification of the CNV leakage area at day 7 (n = 10–16 eyes per group). **d** Quantification of the CNV leakage area at day 14 (n = 14–16 eyes per group). **e** Representative immunofluorescence images of retinal pigment epithelium (RPE)-choroid-sclera flat mounts stained with C5b9 and treated three days after laser-induced CNV. Scale bars, 50 μm. **f** Quantification of the CNV volume in **e**, calculated as CD31+ volume at the site of laser photocoagulation three days after laser-induced CNV (n = 9–15 eyes per group). **g** Quantification of the membrane attack complex (MAC) infiltration volume in **e**, calculated as C5b9+ volume at the site of laser photocoagulation three days after laser-induced CNV (n = 8–14 eyes per group). Data are analyzed using one-way analysis of variance for multiple comparisons with Tukey's test among groups in **c**, **d**, **f**, and **g** (*$P < 0.05$, **$P < 0.01$, ***$P < 0.001$, ****$P < 0.0001$). Data are presented as mean ± SD.

$P < 0.0001$), AAV2/8-sFLT-1-P2A-sCD59 (57.4%, $P < 0.0001$), and Conbercept (54.8%, $P < 0.0001$) group compared to AAV2/8-ZsGreen group (Fig. 3f). There were no statistical differences among AAV2/8-PEDF-P2A-sCD59, AAV2/8-sFLT-1-P2A-sCD59 and Conbercept groups. Taken together, a single injection of AAV2/8-PEDF-P2A-sCD59 or AAV2/8-sFLT-1-P2A-sCD59 markedly decreased vascular leakage and macrophage infiltration over the long term. The efficiency of inhibition of CNV development may be comparable between a single injection of AAV2/8-mediated genes and two injections of Conbercept.

Intravitreal delivery of AAV2/8-mediated genes attenuated retinal neovascularization in a *Vldlr*$^{-/-}$ mouse model

The Vldlr mutant (*Vldlr*$^{-/-}$) mouse is a subretinal neovascularization mouse model typically used to study the vascular features of retinal angiomatous proliferation (a subform of AMD) and macular telangiectasia [30]. In the *Vldlr*$^{-/-}$ mouse retina, neovascularization develops from the retinal vasculature to the common avascular photoreceptor layer by P12 and extends to the RPE layer by P16 [31]. Here, *Vldlr*$^{-/-}$ mice were used to test the anti-retinal neovascular effect of AAV2/8-PEDF-P2A-sCD59 and AAV2/8-sFLT-1-P2A-sCD59. Mice were administered AAV2/8-ZsGreen, AAV2/8-PEDF-P2A-sCD59, AAV2/8-sFLT-1-P2A-sCD59, or Conbercept at P12. Retinal flat mounts were stained for CD31 at P26 to validate retinal neovascularization (Fig. 4a, b). Retinal neovascularization was greatly reduced in mice administered AAV2/8-PEDF-P2A-sCD59 (48.8%, $P = 0.0087$), AAV2/8-sFLT-1-P2A-sCD59 (53.3%, $P = 0.0148$), or Conbercept (59.9%, $P = 0.0036$) compared with that in mice administered AAV2/8-ZsGreen. There were no statistical differences between the Conbercept- and AAV2/8-mediated gene therapy groups (Fig. 4c). We also used 4- to 6-week mice to detect the therapeutic effect of our drugs on vascular leakage by FFA (Fig. 4a, b). We evaluated the vascular leakage area and spots 28 days after administration. AAV2/8-PEDF-P2A-sCD59 and AAV2/8-sFLT-1-P2A-sCD59 could significantly reduce vascular leakage compared with AAV2/8-ZsGreen (Fig. 4d, e). In addition, compared with Conbercept, AAV2/8-PEDF-P2A-sCD59 ($P = 0.0116$) and AAV2/8-sFLT-1-P2A-sCD59 ($P = 0.0001$) had more obvious inhibition on the leakage area (Fig. 4d).

Extracellular signal-regulated kinase and nuclear factor-κB pathway activation were downregulated by AAV2/8-mediated gene therapy

To determine the mechanism underlying the antiangiogenic effect of AAV2/8-mediated gene therapy, RNA sequencing (RNA-seq) was used to analyze retina-RPE-choroid complexes from mice with CNV. Enrichment analysis demonstrated that downregulated genes were mainly associated with angiogenesis processes and tumor necrosis factor (Tnf)-α signaling via nuclear factor (NF)-κB in the AAV2/8-PEDF-P2A-sCD59 group compared to that in the AAV2/8-ZsGreen group (Fig. 5a, c, d). A similar result was observed in the AAV2/8-sFLT-1-P2A-sCD59 group (Fig. 5b, e, f).

Endothelial extracellular signal-regulated kinase (ERK) phosphorylation is related to microvascular endothelial proliferation and may be activated by VEGF [32]. Therefore, mouse retinal-RPE-choroid complexes were collected to assess ERK activation under each condition. ERK phosphorylation levels were significantly decreased in the AAV2/8-PEDF-P2A-sCD59-, AAV2/8-sFLT-1-P2A-sCD59-, and Conbercept-treated groups compared with those in the negative control group (Fig. 5h).

Besides VEGF signaling, immune activation is another major pathogenic pathway in AMD [33]. Based on the results of enrichment analysis, the influence of AAV vectors on the inflammatory response in vitro and in vivo was explored. In vitro, inflammatory factors, including p-NF-κB p65, inducible nitric oxide synthase (iNOS), and interleukin (IL)-1β, were examined in BV2 cells using western blotting. These inflammatory indices were downregulated in the AAV2/8-PEDF-P2A-sCD59, AAV2/8-sFLT-1-P2A-sCD59, and the Conbercept groups compared with those in the AAV2/8-ZsGreen group (Fig. 5g). In vivo, protein levels of p-NF-κB p65, NF-κB1 p105, and IL-1β decreased in the AAV2/8-PEDF-P2A-sCD59, AAV2/8-sFLT-1-P2A-sCD59, and Conbercept groups (Fig. 5h). The mRNA expression of inflammatory factors, decreased in the AAV2/8-PEDF-P2A-sCD59, AAV2/8-sFLT-1-P2A-sCD59, and Conbercept groups compared with that in the AAV2/8-ZsGreen group (Fig. 5i–k). Overall, AAV2/8-PEDF-P2A-sCD59 and AAV2/8-sFLT-1-P2A-sCD59 efficiently inhibited neovascularization by downregulating ERK activation and the NF-κB pathway.

Safety of AAV2/8-mediated gene delivery into the eye

The retinal structure of AAV2/8-related treatments was assessed using OCT four weeks after intravitreal injection (Fig. 6a, b). There were no differences in whole retinal thickness between the phosphate-buffered saline (PBS)- and AAV2/8-injected groups (Fig. 6c). Next, the thickness of the retinal nerve fiber layer and ganglion cell-inner plexiform layer (RNFL + GC-IPL), inner nuclear layer (INL), outer nuclear layer (ONL), and outer segment + inner segment + retinal pigment epithelium (OS + IS + RPE) was measured. Marked differences were not observed in each layer between the PBS and AAV2/8-injected eyes (Fig. 6c). To further confirm the safety of AAV, a TUNEL assay was used to assess retinal cell death in mice. Compared to that in the PBS group, almost no TUNEL+ cells were observed in mice injected with AAV vectors, and the number of apoptotic cells was unchanged among the four groups (Fig. 6d).

DISCUSSION

In current nAMD therapies, 40% of patients fail to achieve remission using anti-VEGF monotherapy [34, 35]. Recently, several bispecific fusion proteins showed superior outcomes compared to those of anti-VEGF monotherapy, such as efdamrofusp alfa (code: IBI302), faricimab (RG7716, Roche), and ABBV642. Faricimab and ABBV642 both target VEGF and other angiogenic molecules [36–38]. Efdamrofusp alfa simultaneously inhibits complement system activation and neutralizes VEGF [39]. The agent was verified to be more useful than anti-VEGF monotherapy in preclinical trials and was well tolerated in a Phase I dose-escalating clinical trial [40]. However, for anti-VEGF monotherapy, these protein agents require repeated injections to ameliorate CNV development owing to their short half-lives. The combined effects of AAV2/8-vectored bio-molecules were explored to develop more reliable and efficient treatments.

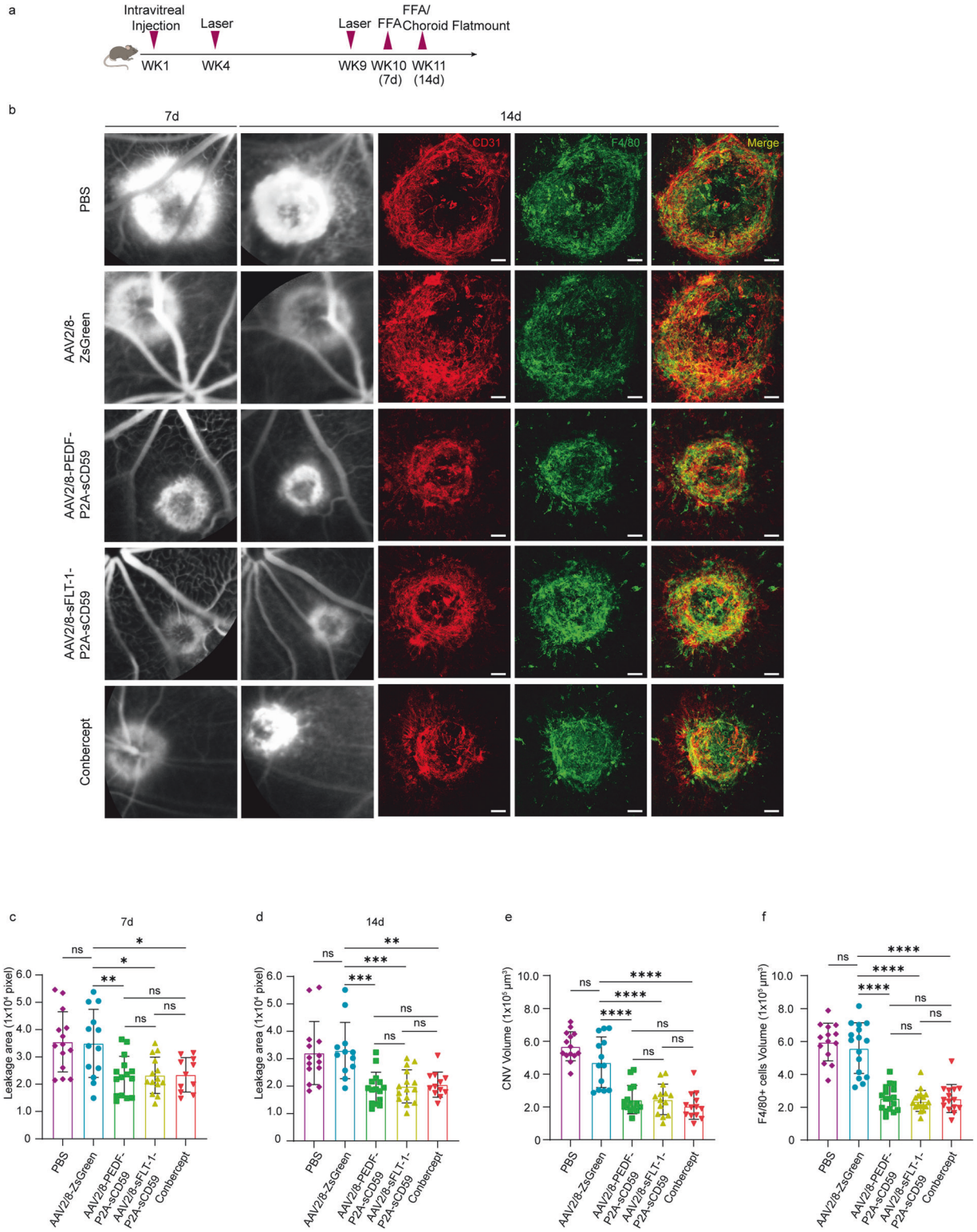

Fig. 3 AAV2/8-mediated gene therapy resulted in long-term inhibition of laser-induced CNV. a Sequential order of intravitreal injections, CNV induction, and analysis. **b** Representative fundus fluorescein angiography (FFA) images showing vascular leakage from mice undergoing the indicated treatment after laser-induced CNV at days 7 and 14 and the representative immunofluorescence images of retinal pigment epithelium (RPE)-choroid-sclera flat mounts stained with CD31 and F4/80. Scale bars, 50 μm. **c** Quantification of the CNV leakage area at day 7 in **b** (n = 11–15 eyes per group). **d** Quantification of the CNV leakage area at day 14 in **b** (n = 12–15 eyes per group). **e** Quantification of the CNV volume in **b**, calculated as CD31+ volume at the site of laser photocoagulation 14 days after laser-induced CNV (n = 13–15 eyes per group). **f** Quantification of the macrophage infiltration volume in **b**, calculated as F4/80+ volume surrounding the CNV lesion 14 days after laser-induced CNV (n = 14–17 eyes per group). Data are analyzed using one-way analysis of variance for multiple comparisons with Tukey's test among groups in **c**–**f** (*$P < 0.05$, **$P < 0.01$, ***$P < 0.001$, ****$P < 0.0001$). Data are presented as mean ± SD.

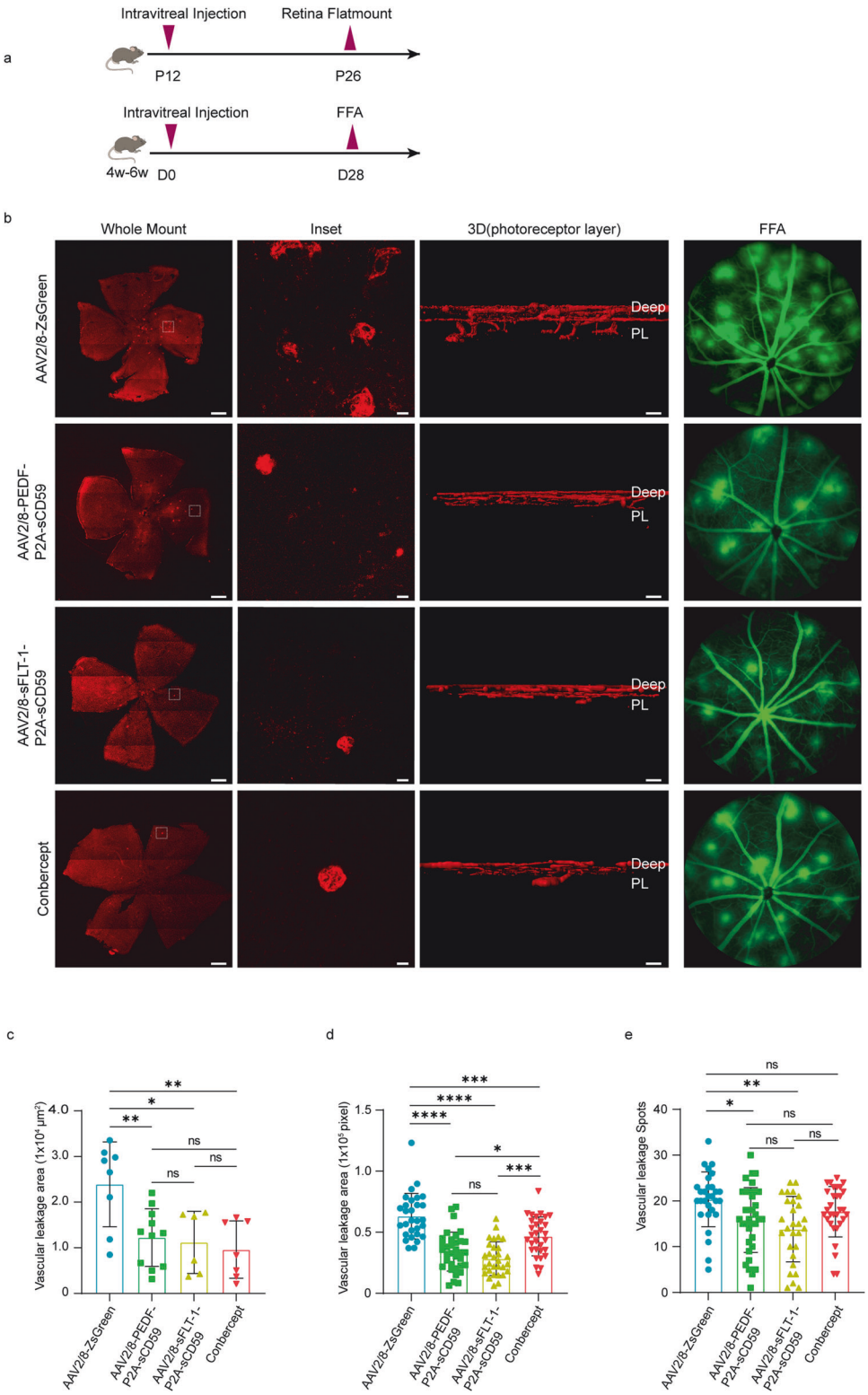

Fig. 4 Intravitreal delivery of AAV2/8-mediated genes attenuated retinal neovascularization in a *Vldlr*$^{-/-}$ mouse model. a Sequential order of intravitreal injections and retina analysis. **b** Representative immunofluorescence images of retinal flat mounts stained with CD31 and representative fundus fluorescein angiography (FFA) images showing vascular leakage from mice aged 4–6 weeks undergoing indicated treatment at day 28. Scale bars, 500 μm in the left row, 20 μm in the middle row, and 30 μm in the right row. **c** Quantification of the vascular leakage area shown in **b** (n = 6–11 eyes per group). **d**, **e** Quantification of the vascular leakage area and spots of **b** (n = 28-34 eyes per group). Data are analyzed using one-way analysis of variance for multiple comparisons with Tukey's test among groups in **c**–**e** (*$P < 0.05$, **$P < 0.01$, ***$P < 0.001$, ****$P < 0.0001$). Data are presented as mean ± SD.

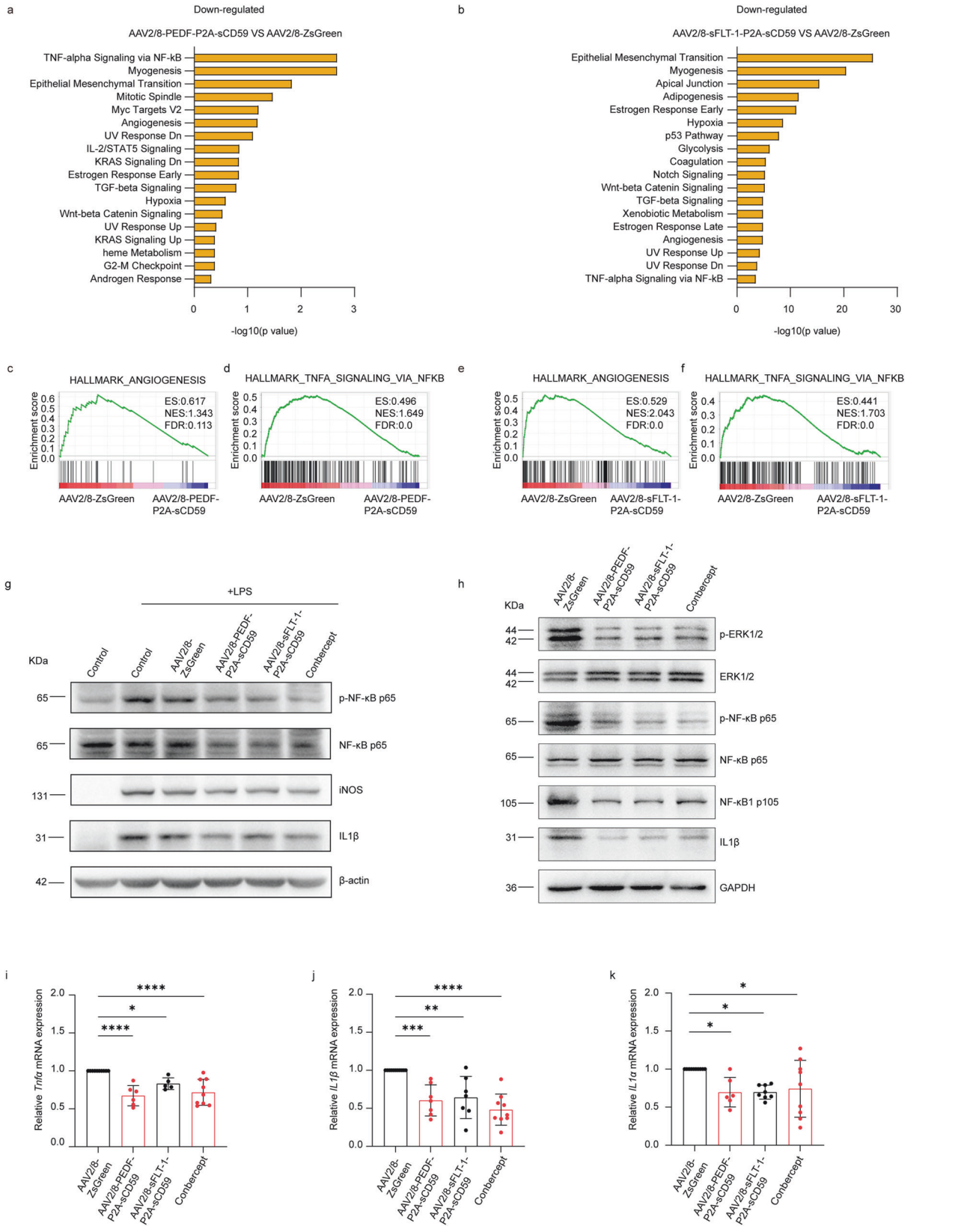

In addition to VEGF, inflammatory responses and complement activation play important roles in CNV development. Various promising molecules have been used for AMD gene therapy. sFLT-1 directly binds to VEGF and forms inactive heterodimers with the fms-like tyrosine kinase receptor KDR/Flk-1-a clinical trial of rAAV.sFLT-1 (NCT01024998) has shown safe and long-term efficacy in patients with nAMD [14, 41–43]. PEDF is a multifunction protein and plays a critical role in pathophysiological processes,

Fig. 5 Extracellular signal-regulated kinase and nuclear factor-κB pathway activation were downregulated by AAV2/8-mediated gene therapy. a RNA-sequencing (RNA-seq) analysis of retina-choroid complexes from AAV2/8-PEDF-P2A-sCD59- and AAV2/8-ZsGreen-treated mice three days after laser induction and enrichment analysis of the significantly downregulated genes in AAV2/8-PEDF-P2A-sCD59-treated mice. **b** RNA-seq analysis of retina-choroid complexes from AAV2/8-sFLT-1-P2A-sCD59- and AAV2/8-ZsGreen-treated mice three days after laser induction and enrichment analysis of the significantly downregulated genes in AAV2/8-sFLT-1-P2A-sCD59-treated mice. **c**, **d** Gene set enrichment analysis (GSEA) of HALLMARK_ANGIOGENESIS and HALLMARK_TNFA_SIGNALING_VIA_NFκB in the retina-choroid complex of AAV2/8-PEDF-P2A-sCD59- and AAV2/8-ZsGreen-treated mice. **e**, **f** GSEA of HALLMARK_ANGIOGENESIS and HALLMARK_TNFA_SIGNALING_-VIA_NFκB in the retina-choroid complex of AAV2/8-sFLT-1-P2A-sCD59- and AAV2/8-ZsGreen-treated mice. **g** BV2 cells were pretreated with AAV2/8-ZsGreen, AAV2/8-PEDF-P2A-sCD59, AAV2/8-sFLT-1-P2A-sCD59, or Conbercept and then stimulated with lipopolysaccharide (LPS). Western blot showing expression levels of p-NF-κB p65/NF-κB p65, inducible nitric oxide synthase (iNOS), and IL-1β. **h** Western blotting of p-ERK/ERK, p-NF-κB p65/NF-κB p65, NF-κB1 p105 and IL-1β in the retina-choroid complex of AAV2/8-ZsGreen-, AAV2/8-PEDF-P2A-sCD59-, AAV2/8-sFLT-1-P2A-sCD59-, and Conbercept-treated mice three days after laser photocoagulation and quantification. (i-k) Quantitative reverse transcription-polymerase chain reaction (qRT-PCR) analysis of the mRNA expression of tumor necrosis factor (Tnf)α, interleukin (IL)-1α and IL-1β in the retina-choroid complex of AAV2/8-ZsGreen-, AAV2/8-PEDF-P2A-sCD59-, AAV2/8-sFLT-1-P2A-sCD59-, and Conbercept-treated mice three days after laser photocoagulation (n = 5–11 eyes per group). In all panels: $^{*}P < 0.05$, $^{**}P < 0.01$, $^{***}P < 0.001$, $^{****}P < 0.0001$. Values represent one-way analysis of variance multiple comparisons with Tukey's test among groups in **i**, **j**, and **k**. Data are presented as mean ± SD.

such as angiogenesis, inflammation, and neuroprotection [16, 44–47]. AdGVPEDF.11D (NCT00109499) used a replication-deficient adenoviral vector carrying PEDF to treat angiogenesis. GenVec's Phase I clinical trial showed no severe adverse complications in patients' eyes, except for transient intraocular inflammation [48]. MAC deposits on the normal human choriocapillaris and will heavily deposit on the choroidal neovascular of nAMD patients [49]. Components of the sublytic MAC promote VEGF expression and CNV development [17]. In the process of complement activation, other complement molecules also promote the development of CNV, such as anaphylatoxins and C3 molecules upstream of MAC. However, these proteins in the complement system play important roles in immune surveillance and tissue homeostasis. Reduced levels of these proteins can be detrimental to the long-term health of the retina. For example, in a clinical trial (FILLY, NCT02503332) for the treatment of geographical atrophy, inhibition of C3 induced nAMD in 18% of treated eyes, higher than the control eyes (1%) [50]. The result showed that inhibition of complement activation is important in AMD, but direct inhibition of C3 levels may be harmful in some patients. Therefore, it is more appropriate to reduce MAC below the pathological level, in line with the normal physiological process of the aging retina. CD59 inhibits MAC formation by binding to the C5b678 terminal complement protein and C9 during MAC assembly [51]. sCD59 is a non-membrane-binding isoform of CD59 formed by deleting the GPI membrane anchor [52, 53]. In a preclinical study, AdCAGsCD59 attenuated CNV and MAC formation in mice [54]. Currently, two clinical studies on AdCAGsCD59 have been conducted for the treatment of dry (NCT03144999) and wet AMD (NCT03585556). Therefore, PEDF, sCD59, and sFLT-1 are promising candidates for AMD treatment.

AAV2/8 was used as the delivery platform, and two target genes linked to P2A were simultaneously inserted to separately express these genes. The recombinant AAV vectors had dual inhibitory effects on the complement and inflammatory systems (AAV2/8-PEDF-P2A-sCD59) or complement and VEGF systems (AAV2/8-sFLT-1-P2A-sCD59). In the nAMD model, a single injection of the AAV vectors showed a long-term efficiency comparable to two injections of Conbercept. Compared to the strong immune response of adenoviral vectors and the integration of the lentiviruses into the host genome, AAV2/8 vectors showed low immunogenicity and good safety in the retina [55, 56]. In conclusion, these AAV2/8 vectors had the advantages of long-term expression, targeting multiple pathways, good safety, and strong inhibition of CNV, making them promising therapeutic candidates.

sFLT-1 prevents VEGFA from binding to the VEGF receptor, blocking subsequent signal transduction. CD59 can inhibit complement activation through preventing the MAC formation, subsequently reducing inflammation in AMD [57]. PEDF suppresses angiogenesis by inhibiting the activity of angiogenesis factors VEGF and FGF2 [44]. It also inhibits the proliferation and migration of endothelial cells (ECs) and induces apoptosis of ECs through the FAS/FASL signaling pathway [58, 59]. Both AAV2/8-sFLT-1-P2A-sCD59 and AAV2/8-PEDF-P2A-sCD59 exhibit functions of anti-VEGF, anti-complement activation, and anti-inflammatory effects in the treatment of AMD.

In our study, we found that both AAV2/8-sFLT-1-P2A-sCD59 and AAV2/8-PEDF-P2A-sCD59 could significantly downregulate ERK and NF-κB pathway activation in the CNV model. VEGF binds to VEGFR2, resulting in the activation of the mitogen-activated protein kinase (ERK1/2) signaling pathway. The VEGF-activated ERK1/2 pathway is essential in vascular proliferation and differentiation [60, 61]. Proinflammatory cytokine production and inflammatory response activation regulated by NF-κB effectively promote the development of nAMD [62–65]. Previous studies have reported the close relationship between these target genes (sFLT-1, PEDF, and sCD59) and the NF-κB/ERK pathway. sFLT-1 blocks angiogenic effects by binding to VEGF and forming a heterodimer with VEGFR-1 [66]. Competitive inhibition of VEGF-VEGFR-2 binding through PEDF effectively inhibited permeability and angiogenesis of retinal endothelial cells [67]. PEDF interacts with adipose triglyceride lipase in endothelial cells to inhibit angiogenesis by upregulating FasL expression through the NF-κB pathway [68]. The MAC might interact with signal molecules to promote the expression of secondary messengers that activate proliferative and proinflammatory pathways, such as ERK and NF-κB signaling. MAC deposition may promote inflammasome assembly and release of inflammatory factors (IL-1, IL-18, IL-1α, and Tnf) through NF-κB-dependent transcription [69]. sCD59 competitively inhibited MAC formation, which might contribute to the downregulation of the NF-κB and ERK pathways. Therefore, AAV2/8-sFLT-1-P2A-sCD59 and AAV2/8-PEDF-P2A-sCD59 had more thorough inhibition of CNV in vascular proliferation and inflammation through the synergistic effect of multiple targets. In this study, ERK and NF-κB pathway activation was significantly downregulated by AAV vectors in the CNV model, consistent with the results of previous studies.

In conclusion, two gene therapy agents, AAV2/8-PEDF-P2A-sCD59 and AAV2/8-sFLT-1-P2A-sCD59 were generated, targeting both the anti-angiogenic and complement systems for the treatment of nAMD. Through intravitreal administration, AAV2/8-PEDF-P2A-sCD59 and AAV2/8-sFLT-1-P2A-sCD59 effectively attenuated neovascularization in CNV and *Vldlr*$^{-/-}$ mouse models and produced long-lasting therapeutic effects comparable to that of two injections of Conbercept in the CNV model. The AAV2/8-mediated genes suppressed ERK and NF-κB activation, resulting in antiangiogenic activity. Thus, this study demonstrates the long-term therapeutic effects and safety of AAV2/8-based multi-target gene therapy for the treatment of nAMD.

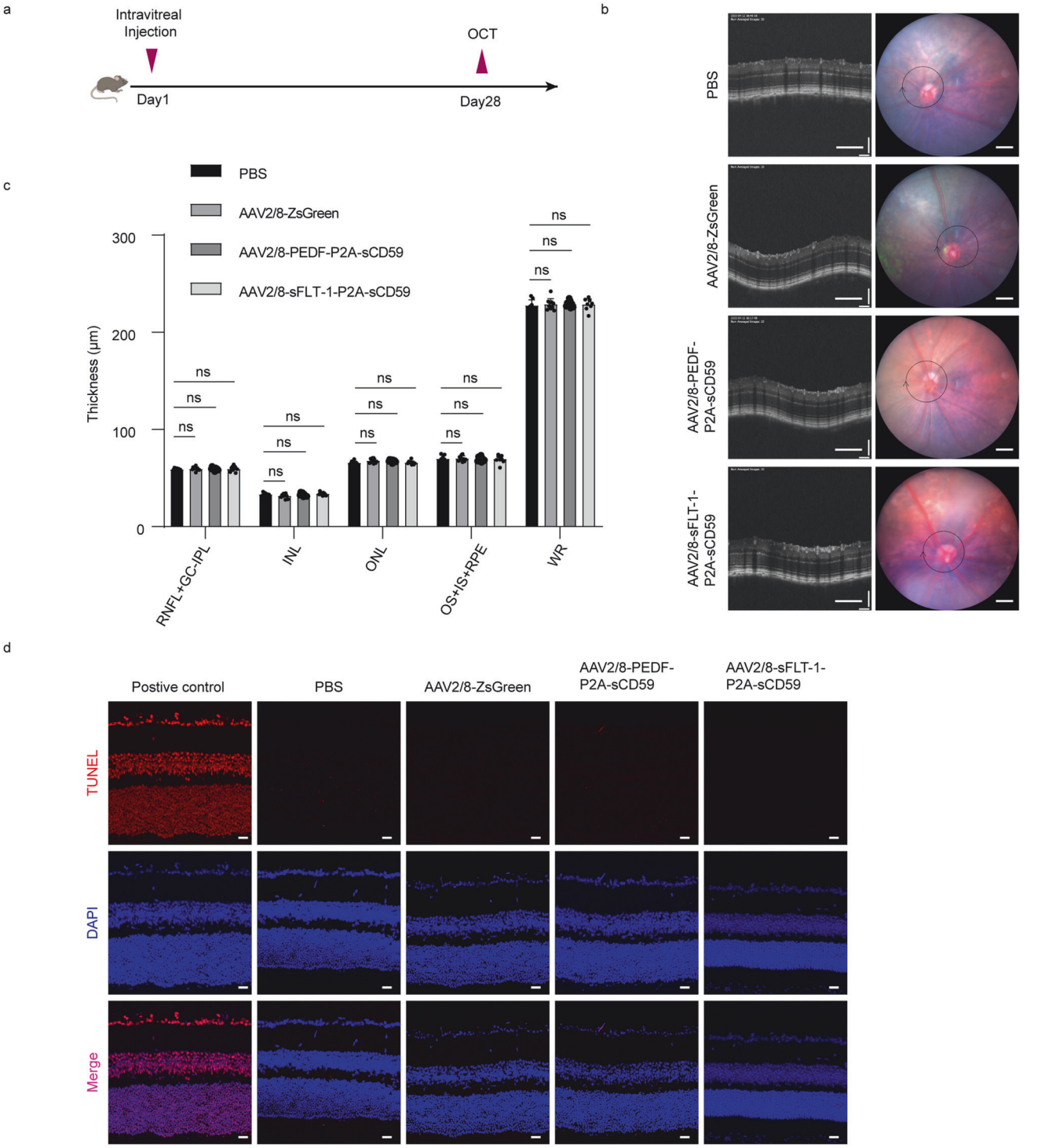

Fig. 6 Safety of AAV2/8-mediated gene delivery into the eye. a Sequential order of intravitreal injections and optical coherence tomography (OCT) analysis. **b** Retinal thickness 28 days after intravitreal injection of phosphate-buffered saline (PBS), AAV2/8-ZsGreen, AAV2/8-PEDF-P2A-sCD59, and AAV2/8-sFLT-1-P2A-sCD59 visualized using OCT. Scale bars, 200 μm in the first row, 300 μm in the next row. **c** Quantification of RNFL + GC-IPL, ONL, INL, OS + IS + RPE, and WR (n = 8–10 eyes per group) 28 days after intravitreal injection. **d** Representative immunofluorescence images showing terminal deoxynucleotidyl transferase dUTP nick end labeling (TUNEL) + cells (TUNEL, red) in the retina. Scale bars, 20 μm. In all panels: $^{*}P < 0.05$, $^{**}P < 0.01$, $^{***}P < 0.001$, $^{****}P < 0.0001$. Values represent one-way analysis of variance for multiple comparisons with Tukey's test among groups in **c**. Data are presented as mean ± SD. RNFL retinal nerve fiber layer, GC-IPL ganglion cell-inner plexiform layer, INL inner nuclear layer, ONL outer nuclear layer, OS outer segment, IS inner segment, RPE retinal pigment epithelium, WR whole retina.

DATA AVAILABILITY

All data used in this paper has been presented in the figures.

REFERENCES

1. Wong WL, Su X, Li X, Cheung CMG, Klein R, Cheng C-Y, et al. Global prevalence of age-related macular degeneration and disease burden projection for 2020 and 2040: a systematic review and meta-analysis. Lancet Glob Health. 2014;2:e106–e116.
2. Fleckenstein M, Keenan TD, Guymer RH, Chakravarthy U, Schmitz-Valckenberg S, Klaver CC, et al. Age-related macular degeneration. Nat Rev Dis Prim. 2021;7:31.
3. Holz FG, Figueroa MS, Bandello F, Yang Y, Ohji M, Dai H, et al. Ranibizumab treatment in treatment-naive neovascular age-related macular degeneration: results from LUMINOUS, a global real-world study. Retina. 2020;40:1673–85.
4. Gonzalez VH, Campbell J, Holekamp NM, Kiss S, Loewenstein A, Augustin AJ, et al. Early and long-term responses to anti–vascular endothelial growth factor therapy in diabetic macular edema: analysis of protocol I data. Am J Ophthalmol. 2016;172:72–79.
5. MASON JO III, White MF, Feist RM, Thomley ML, Albert MA, Persaud TO, et al. Incidence of acute onset endophthalmitis following intravitreal bevacizumab (Avastin) injection. Retina 2008;28:564–7.
6. Heier JS, Brown DM, Chong V, Korobelnik J-F, Kaiser PK, Nguyen QD, et al. Intravitreal aflibercept (VEGF trap-eye) in wet age-related macular degeneration. Ophthalmology. 2012;119:2537–48.
7. Mehta H, Tufail A, Daien V, Lee AY, Nguyen V, Ozturk M, et al. Real-world outcomes in patients with neovascular age-related macular degeneration treated with intravitreal vascular endothelial growth factor inhibitors. Prog Retinal Eye Res. 2018;65:127–46.
8. Martin DF, Maguire MG, Ying Ga, Grunwald JE, Fine SL, Jaffe GJ. Ranibizumab and bevacizumab for neovascular age-related macular degeneration. N Engl J Med. 2011;364:1897–908.
9. Nonnenmacher M, Weber T. Intracellular transport of recombinant adeno-associated virus vectors. Gene Ther. 2012;19:649–58.
10. Wang D, Tai PW, Gao G. Adeno-associated virus vector as a platform for gene therapy delivery. Nat Rev Drug Discov. 2019;18:358–78.
11. Khanani AM, Kiss S, Turpcu A, Hoang C, Osborne A. Phase 1 study of intravitreal gene therapy ADVM-022 for neovascular AMD (OPTIC Trial). Investigative Ophthalmol Vis Sci. 2020;61:1154–1154.
12. Heier J, Campochiaro P, Ho A. Key takeaways from the RGX-314 phase I/IIa clinical trial for wet AMD (Cohorts 1-5). Am Acad Ophthamol. 2019;10:21.
13. Lebherz C, Maguire A, Tang W, Bennett J, Wilson JM. Novel AAV serotypes for improved ocular gene transfer. J gene Med. 2008;10:375–82.
14. Constable IJ, Pierce CM, Lai C-M, Magno AL, Degli-Esposti MA, French MA, et al. Phase 2a randomized clinical trial: safety and post hoc analysis of subretinal rAAV.sFLT-1 for wet age-related macular degeneration. EBioMedicine. 2016;14:168–75.
15. Amaral J, Becerra SP. Effects of human recombinant PEDF protein and PEDF-derived peptide 34-mer on choroidal neovascularization. Investigative Ophthalmol Vis Sci. 2010;51:1318–26.
16. Tombran-Tink J, Chader GG, Johnson LV. PEDF: a pigment epithelium-derived factor with potent neuronal differentiative activity. Exp eye Res. 1991;53:411–4.
17. Kunchithapautham K, Rohrer B. Sublytic membrane-attack-complex (MAC) activation alters regulated rather than constitutive vascular endothelial growth factor (VEGF) secretion in retinal pigment epithelium monolayers. J Biol Chem. 2011;286:23717–24.
18. Cui B, Guo X, Zhou W, Zhang X, He K, Bai T, et al. Exercise alleviates neovascular age-related macular degeneration by inhibiting AIM2 inflammasome in myeloid cells. Metabolism. 2023;144:155584.
19. Livak KJ, Schmittgen TD. Analysis of relative gene expression data using real-time quantitative PCR and the 2− ΔΔCT method. Methods. 2001;25:402–8.
20. Chen EY, Tan CM, Kou Y, Duan Q, Wang Z, Meirelles GV, et al. Enrichr: interactive and collaborative HTML5 gene list enrichment analysis tool. BMC Bioinforma. 2013;14:1–14.
21. Kuleshov MV, Jones MR, Rouillard AD, Fernandez NF, Duan Q, Wang Z, et al. Enrichr: a comprehensive gene set enrichment analysis web server 2016 update. Nucleic Acids Res. 2016;44:W90–W97.
22. Xie Z, Bailey A, Kuleshov MV, Clarke DJ, Evangelista JE, Jenkins SL, et al. Gene set knowledge discovery with Enrichr. Curr Protoc. 2021;1:e90.
23. Subramanian A, Tamayo P, Mootha VK, Mukherjee S, Ebert BL, Gillette MA, et al. Gene set enrichment analysis: a knowledge-based approach for interpreting genome-wide expression profiles. Proc Natl Acad Sci. 2005;102:15545–50.
24. Liberzon A, Subramanian A, Pinchback R, Thorvaldsdóttir H, Tamayo P, Mesirov JP. Molecular signatures database (MSigDB) 3.0. Bioinformatics. 2011;27:1739–40.
25. Liberzon A, Birger C, Thorvaldsdóttir H, Ghandi M, Mesirov JP, Tamayo P. The molecular signatures database hallmark gene set collection. Cell Syst. 2015;1:417–25.
26. Ishikawa K, Kannan R, Hinton DR. Molecular mechanisms of subretinal fibrosis in age-related macular degeneration. Exp Eye Res. 2016;142:19–25.
27. Hughes CP, O'Flynn NM, Gatherer M, McClements ME, Scott JA, MacLaren RE, et al. AAV2/8 anti-angiogenic gene therapy using single-chain antibodies inhibits murine choroidal neovascularization. Mol Ther Methods Clin Dev. 2019;13:86–98.
28. Patel M, Chan C-C. Immunopathological aspects of age-related macular degeneration. Semin Immunopathol. 2008;30:97–110.
29. Dastgheib K, Green WR. Granulomatous reaction to Bruch's membrane in age-related macular degeneration. Arch Ophthalmol. 1994;112:813–8.
30. Usui-Ouchi A, Usui Y, Kurihara T, Aguilar E, Dorrell MI, Ideguchi Y, et al. Retinal microglia are critical for subretinal neovascular formation. JCI insight. 2020;5:e137317.
31. Sun Y, Lin Z, Liu C-H, Gong Y, Liegl R, Fredrick TW, et al. Inflammatory signals from photoreceptor modulate pathological retinal angiogenesis via c-Fos. J Exp Med. 2017;214:1753–67.
32. Simons M, Eichmann A. Molecular controls of arterial morphogenesis. Circulation Res. 2015;116:1712–24.
33. Zhang Y, Wong WT. Innate immunity in age-related macular degeneration. Age Relat Macular Degeneration. 2021;1256:121–41.
34. Yang S, Zhao J, Sun X. Resistance to anti-VEGF therapy in neovascular age-related macular degeneration: a comprehensive review. Drug Des Dev Ther. 2016;10:1857–67.
35. Tranos P, Vacalis A, Asteriadis S, Koukoula S, Vachtsevanos A, Perganta G, et al. Resistance to antivascular endothelial growth factor treatment in age-related macular degeneration. Drug Des Dev Ther. 2013;7:485–90.
36. Regula JT, Lundh von Leithner P, Foxton R, Barathi VA, Cheung CMG, Bo Tun SB, et al. Targeting key angiogenic pathways with a bispecific Cross MA b optimized for neovascular eye diseases. EMBO Mol Med. 2016;8:1265–88.
37. Chakravarthy U, Bailey C, Brown D, Campochiaro P, Chittum M, Csaky K, et al. Phase I trial of anti–vascular endothelial growth factor/anti-angiopoietin 2 bispecific antibody RG7716 for neovascular age-related macular degeneration. Ophthalmol Retin. 2017;1:474–85.
38. Ding K, Eaton L, Bowley D, Rieser M, Chang Q, Harris MC, et al. Generation and characterization of ABBV642, a dual variable domain immunoglobulin molecule (DVD-Ig) that potently neutralizes VEGF and PDGF-BB and is designed for the treatment of exudative age-related macular degeneration. MAbs. 2017;9:269–84.
39. Ren X, Li J, Xu X, Wang C, Cheng Y. IBI302, a promising candidate for AMD treatment, targeting both the VEGF and complement system with high binding affinity in vitro and effective targeting of the ocular tissue in healthy rhesus monkeys. Exp Eye Res. 2016;145:352–8.
40. Yang S, Li T, Jia H, Gao M, Li Y, Wan X, et al. Targeting C3b/C4b and VEGF with a bispecific fusion protein optimized for neovascular age-related macular degeneration therapy. Sci Transl Med. 2022;14:eabj2177.
41. Kendall RL, Thomas KA. Inhibition of vascular endothelial cell growth factor activity by an endogenously encoded soluble receptor. Proc Natl Acad Sci. 1993;90:10705–9.
42. Kendall RL, Wang G, Thomas KA. Identification of a natural soluble form of the vascular endothelial growth factor receptor, FLT-1, and its heterodimerization with KDR. Biochem Biophys Res Commun. 1996;226:324–8.
43. Heier JS, Kherani S, Desai S, Dugel P, Kaushal S, Cheng SH, et al. Intravitreous injection of AAV2-sFLT01 in patients with advanced neovascular age-related macular degeneration: a phase 1, open-label trial. Lancet. 2017;390:50–61.
44. Dawson D, Volpert O, Gillis P, Crawford S, Xu H-J, Benedict W, et al. Pigment epithelium-derived factor: a potent inhibitor of angiogenesis. Science. 1999;285:245–8.
45. Wang JJ, Zhang SX, Mott R, Chen Y, Knapp RR, Cao W, et al. Anti-inflammatory effects of pigment epithelium-derived factor in diabetic nephropathy. Am J Physiol Ren Physiol. 2008;294:F1166–F1173.
46. Zhang SX, Wang JJ, Dashti A, Wilson K, Zou M-H, Szweda L, et al. Pigment epithelium-derived factor mitigates inflammation and oxidative stress in retinal pericytes exposed to oxidized low-density lipoprotein. J Mol Endocrinol. 2008;41:135–43.
47. He X, Cheng R, Benyajati S, Ma J-x. PEDF and its roles in physiological and pathological conditions: implication in diabetic and hypoxia-induced angiogenic diseases. Clin Sci. 2015;128:805–23.
48. Campochiaro PA, Nguyen QD, Shah SM, Klein ML, Holz E, Frank RN, et al. Adenoviral vector-delivered pigment epithelium-derived factor for neovascular age-related macular degeneration: results of a phase I clinical trial. Hum Gene Ther. 2006;17:167–76.
49. Zeng S, Whitmore SS, Sohn EH, Riker MJ, Wiley LA, Scheetz TE, et al. Molecular response of chorioretinal endothelial cells to complement injury: implications for macular degeneration. J Pathol. 2016;238:446–56.
50. Liao DS, Metlapally R, Joshi P. Pegcetacoplan treatment for geographic atrophy due to age-related macular degeneration: a plain language summary of the FILLY study. Immunotherapy. 2022;14:995–1006.
51. Rollins SA, Sims P. The complement-inhibitory activity of CD59 resides in its capacity to block incorporation of C9 into membrane C5b-9. J Immunol. 1990;144:3478–83.

52. Lehto T, Meri S. Interactions of soluble CD59 with the terminal complement complexes. CD59 and C9 compete for a nascent epitope on C8. J Immunol. 1993;151:4941–9.
53. Sugita Y, Ito K, Shiozuka K, Suzuki H, Gushima H, Tomita M, et al. Recombinant soluble CD59 inhibits reactive haemolysis with complement. Immunology. 1994;82:34.
54. Cashman SM, Ramo K, Kumar-Singh R. A non membrane-targeted human soluble CD59 attenuates choroidal neovascularization in a model of age related macular degeneration. PloS One. 2011;6:e19078.
55. Muruve DA. The innate immune response to adenovirus vectors. Hum Gene Ther. 2004;15:1157–66.
56. Moiani A, Paleari Y, Sartori D, Mezzadra R, Miccio A, Cattoglio C, et al. Lentiviral vector integration in the human genome induces alternative splicing and generates aberrant transcripts. J Clin Investig. 2012;122:1653–66.
57. Morgan BP. Complement membrane attack on nucleated cells: resistance, recovery and non-lethal effects. Biochem J. 1989;264:1.
58. Barnstable CJ, Tombran-Tink J. Neuroprotective and antiangiogenic actions of PEDF in the eye: molecular targets and therapeutic potential. Prog Retinal Eye Res. 2004;23:561–77.
59. Farnoodian M, Wang S, Dietz J, Nickells RW, Sorenson CM, Sheibani N. Negative regulators of angiogenesis: important targets for treatment of exudative AMD. Clin Sci. 2017;131:1763–80.
60. Koch S, Tugues S, Li X, Gualandi L, Claesson-Welsh L. Signal transduction by vascular endothelial growth factor receptors. Biochem J. 2011;437:169–83.
61. Sakurai Y, Ohgimoto K, Kataoka Y, Yoshida N, Shibuya M. Essential role of Flk-1 (VEGF receptor 2) tyrosine residue 1173 in vasculogenesis in mice. Proc Natl Acad Sci. 2005;102:1076–81.
62. Gao J, Liu RT, Cao S, Cui JZ, Wang A, To E, et al. NLRP3 inflammasome: activation and regulation in age-related macular degeneration. Mediators Inflamm. 2015;2015:690243.
63. Lilley E, Stanford SC, Kendall DE, Alexander SP, Cirino G, Docherty JR, et al. ARRIVE 2.0 and the British Journal of Pharmacology: Updated guidance for 2020. Br J Pharmacol. 2020;177:3611.
64. Tarallo V, Hirano Y, Gelfand BD, Dridi S, Kerur N, Kim Y, et al. DICER1 loss and Alu RNA induce age-related macular degeneration via the NLRP3 inflammasome and MyD88. Cell. 2012;149:847–59.
65. Hikage F, Lennikov A, Mukwaya A, Lachota M, Ida Y, Utheim TP, et al. NF-κB activation in retinal microglia is involved in the inflammatory and neovascularization signaling in laser-induced choroidal neovascularization in mice. Exp Cell Res. 2021;403:112581.
66. Charnock-Jones DS. Placental hypoxia, endoplasmic reticulum stress and maternal endothelial sensitisation by sFLT1 in pre-eclampsia. J Reprod Immunol. 2016;114:81–85.
67. Zhang SX, Wang JJ, Gao G, Parke K, Ma J-x. Pigment epithelium-derived factor downregulates vascular endothelial growth factor (VEGF) expression and inhibits VEGF–VEGF receptor 2 binding in diabetic retinopathy. J Mol Endocrinol. 2006;37:1–12.
68. Xu M, Chen X, Yu Z, Li X. Receptors that bind to PEDF and their therapeutic roles in retinal diseases. Front Endocrinol. 2023;14:1116136.
69. Xie CB, Jane-Wit D, Pober JS. Complement membrane attack complex: new roles, mechanisms of action, and therapeutic targets. Am J Pathol. 2020;190:1138–50.

AUTHOR CONTRIBUTIONS

DZ and HY conceived the project, designed the study, and acquired funding. DZ, HY, XW supervised the study. TB, SC, YZ, DL, MX, YG, MD performed the research and analyzed the data. TB, BC, DZ, XW, and HY wrote the manuscript. All the authors reviewed the paper and approved the final draft of the manuscript.

FUNDING

This work was supported by the National Key Research and Development Program of China (2021YFC2401404) and the National Natural Science Foundation of China (82020108007, 82330031, 32070926, 82122018).

COMPETING INTERESTS

The authors declare no competing interests.

ETHICS APPROVAL

No human samples were used in the study. The animal experiments were approved by the Institutional Animal Care and Use Committee of Tianjin Medical University (TMUaMEC 2022006).

ADDITIONAL INFORMATION

Correspondence and requests for materials should be addressed to Xiaohong Wang, Dongming Zhou or Hua Yan.